The microphysical properties of ice fog measured in urban environments of Interior Alaska

Carl G. Schmitt,[1] Martin Stuefer,[2] Andrew J. Heymsfield,[1] and Chang Ki Kim[2]

[1]   The microphysical properties of ice fog were measured at two sites during a small field campaign in January and February of 2012 in Interior Alaska. The National Center for Atmospheric Research Video Ice Particle Sampler probe and Formvar (polyvinyl formal)-coated microscope slides were used to sample airborne ice particles at two polluted sites in the Fairbanks region. Both sites were significantly influenced by anthropogenic emission and additional water vapor from nearby open water power plant cooling ponds. Measurements show that ice fog particles were generally droxtal shaped (faceted, quasi-spherical) for sub-10 µm particles, while plate-shaped crystals were the most frequently observed particles between 10 and 50 µm. A visibility cutoff of 3 km was used to separate ice fog events from other observations which were significantly influenced by larger (50–150 µm) diamond dust particles. The purpose of this study is to more realistically characterize ice fog microphysical properties in order to facilitate better model predictions of the onset of ice fog in polluted environments. Parameterizations for mass and projected area are developed and used to estimate particle terminal velocity. Dimensional characteristics are based on particle geometry and indicated that ice fog particles have significantly lower densities than water droplets as well as reduced cross-sectional areas, the net result being that terminal velocities are estimated to be less than half the value of those calculated for water droplets. Particle size distributions are characterized using gamma functions and have a shape factor (µ) of between −0.5 and −1.0 for polluted ice fog conditions.

1.   Introduction

[2]   In the Arctic winter, strong surface temperature inversions commonly form due to radiative cooling in combination with minimal solar radiation input. This leads to a cold stable boundary layer which inhibits the vertical exchange of aerosols with the free atmosphere and can lead to continuous formation of atmospheric ice crystals. Pollution particles and water vapor produced by power plants and vehicle fuel combustion are easily trapped below the inversion layers. Ice fog can be significantly enhanced by higher aerosol concentrations and increased vapor from these anthropogenic sources. The occurrence of ice fog can seriously impact local populations by reducing daytime temperatures and decreasing visibility, affecting airport operations and vehicular travel. The purpose of this study is to derive a set of microphysical parameterizations to better describe ice fog in models for improved forecasting.

[3]   *Curry et al*. [1990] stated that the main formation mechanism of ice fog and diamond dust is the advection of warmer air from the midlatitudes, which subsequently radiatively cools on cloud-free nights. *Wendler* [1969] suggested that in polluted environments, additional moisture sources for ice fog include automobiles, power plants, and household heating. *Kumai* [1966] showed that 90% of ice fog particles had nuclei which were combustion products. *Benson* [1970] calculated that 4×10^6 kg of water vapor per day was released into the atmosphere in the city of Fairbanks, and as this study is more than 40 years old, it is likely that vapor emissions are much higher today. In the period between 1950 and 1970, the population of Fairbanks tripled and then doubled again by 2010. Figure 1 shows ice fog in the Fairbanks region during prime ice fog formation conditions. Exhaust plumes from vehicles and power plants dissipate very slowly during adding to the ice fog. The significant increase in population has been accompanied by an inevitable increase in vehicular traffic and power plant activity in the Fairbanks area.

[4]   The quantitative distinction differentiating ice fog from diamond dust is very subjective [*Girard and Blanchet*, 2001]. *Girard and Blanchet* [2001] used a particle size cutoff (30 µm) as well as a particle number concentration to distinguish the two types of cloud. Data from this study indicate that there are two distinct populations of atmospheric ice crystals. Observed diamond dust crystals were generally

[1]National Center for Atmospheric Research, Boulder, Colorado, USA.
[2]Geophysical Institute, University of Alaska Fairbanks, Fairbanks, Alaska, USA.

Corresponding author: C. G. Schmitt, National Center for Atmospheric Research, 3450 Mitchell Lane, Boulder, CO 80301, USA. (schmittc@ucar.edu)

Figure 1. Images of ice fog during measurement period on 28 January 2012 in Fairbanks, Alaska. The temperature was approximately −44°C and the NWS visibility was around 0.8 km. (a) Power plant in the background and vehicle exhaust plume. (b) Ice fog near open water cooling pond at Eielson Air Force Base. At the time the photograph was taken, VIPS was in photographed fog bank while the meteorological instrumentation at the north end of the runway was in clear air demonstrating the local inhomogeneity of the fog. (c) Ice fog over the city of Fairbanks. The strong inversion capping the fog can be seen to be very thin as the tops of some trees appear to be out of the fog. Photos were taken at 11:10, 12:56, and 9:40, respectively, on 28 January 2012.

large (20 to 200 µm) plate-shaped crystals with some irregular particles as well as some aggregates. Ice fog particles were generally small (<30 µm) quasi-spherical (droxtal)-shaped particles which only occurred when there was a very strong near-surface inversion. The two cloud types could be mixed with a few large diamond dust particles occasionally being seen even in the heaviest ice fog events. Ice fog in the Fairbanks region has been referred to as "ice pollution" which seems appropriate considering that the heaviest fog was extremely localized near heavy pollution sources. In general, the measurements presented in this work are polluted to very polluted cases.

[5] Ice fog microphysical properties have not been studied in interior Alaska for several decades. Measurements of ice fog particles in the Fairbanks area by *Thuman and Robinson* [1954] showed that ice fog particles were often quasi-spherical droxtal-shaped faceted ice crystals with a mean diameter of 13 µm. *Kumai* [1966] observed ice fog particles between 2 and 15 µm in diameter with the mode of the size distribution being near 5 µm and concentrations between 100 and 200 cm^{-3}. *Ohtake and Huffman* [1969] observed ice fog with median particle diameters between 3 and 8 µm and concentrations between 30 and 668 particles per cm^3. These studies

were conducted by collecting particles on microscope slides coated with silicone oil. Slides were examined under a microscope, and sedimentation velocity estimates were used to estimate size distributions and concentrations. An additional study took place in Barrow, Alaska, which was noted by *Gultepe et al.* [2009]. Their measurements of cleaner ice fog showed that particle sizes were generally below 20 µm and particle concentrations ranged from 10 to 100 cm^{-3}.

[6] To date, there are only a few models in existence which are capable of predicting ice fog. No operationally used numerical weather prediction (NWP) model represents ice fog in a realistic manner. Ice fog typically forms in shallow layers within the atmospheric winter boundary layer, which is characterized by strong temperature inversions and low wind conditions. In order to model ice fog events, we need (a) a realistic representation of the temperature inversions and more accurate parameterization schemes describing the soil-atmosphere interactions, (b) a realistic representation of the physics and the chemical characteristics of available ice nuclei, and (c) a detailed description of the ice fog particle microphysics. Most NWP models use single moment microphysics neglecting explicit ice particle number concentrations and size spectra. Fog visibility is typically parameterized as a function of relative
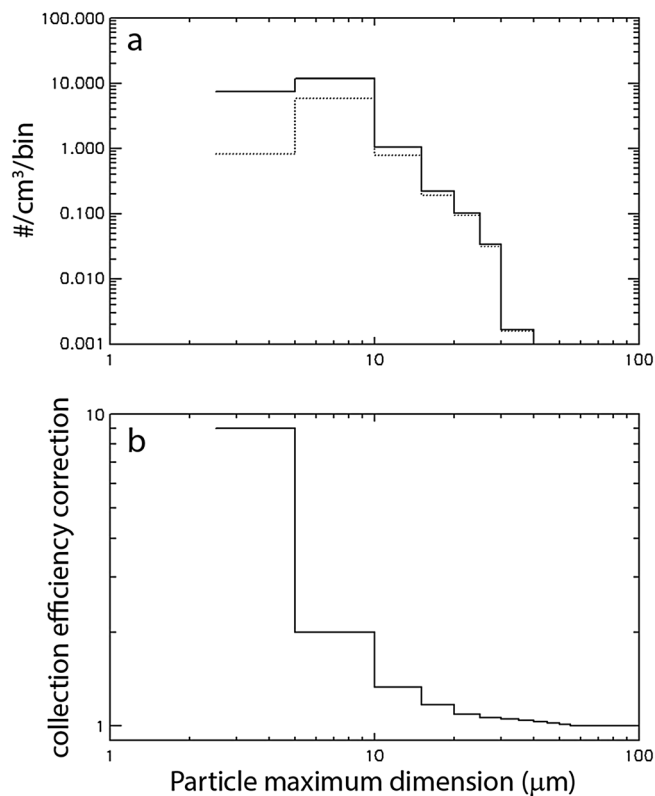
Figure 2. (a) Measured particle size distribution from the VIPS (dotted line) corrected for collection efficiency uncertainties (solid line). Size distribution is from 600 UTC 29 January 2013. (b) Collection efficiency correction factor by size bin for VIPS data. To correct the measured particle size distributions, the measured value is multiplied by the correction factor shown in Figure 2b.

humidity. New efforts are needed to better represent anthropogenic and natural water vapor sources in NWP models.

[7] The results of these microphysical observations of ice fog are being used to improve the prediction of ice fog events using the weather research forecast (WRF) model with a specifically (for ice fog) modified Thompson microphysics scheme [*Thompson et al.*, 2004]. New physically based parameterizations are included in our WRF model setup for simulating homogeneous and heterogeneous ice nucleation, droplet activation, and droplet size distribution. The homogeneous freezing of supercooled liquid water and haze droplets is a dominant process to form ice fog. The double moment Thompson microphysics scheme was modified with ice particle number concentrations, size distributions, and typical settling velocities of ice particles found during our observational period. In addition, surface characteristics were changed in order for WRF to more realistically predict the very stable boundary conditions. The model setup and results will be described in a follow-up publication.

[8] This publication describes microphysical measurements of ice fog particles taken in January and February of 2012 in the highly polluted Fairbanks region. During the observation period, the air temperature dropped to as low as −47°C and dense ice fog decreased the visibility to as low as 0.2 km as reported by the National Weather Service (NWS). In section 2, the ice fog particle observation

instrumentation and analysis techniques will be discussed. Section 3 describes the synoptic conditions that led to the ice fog during the observation period. Section 4 will show results of the observations, including particle size distributions, and particle habit information. The work will be summarized in section 5.

2. Instrumentation and Analysis Techniques

2.1. Instrumentation

[9] The National Center for Atmospheric Research (NCAR) Video Ice Particle Sampler (VIPS) probe was deployed to Fairbanks for ground-based particle sampling of ice fog during the winter of 2012. The VIPS collects and images a continuous sample of cloud particles as small as 3 μm. The VIPS has been used for airborne field campaigns as well as laboratory measurements for many years [*Schmitt and Heymsfield*, 2009; *McFarquhar and Heymsfield*, 1997; *Schön et al.*, 2011]. Particles are collected continuously on a looped, clear plastic belt coated with silicone oil. The portion of the belt exposed to the atmosphere is imaged by a high-resolution video camera. The resulting video imagery is recorded onto a solid-state digital video recorder (DVR). After imaging, particles are scraped off the belt, and oil is reapplied before passing through the sample inlet again. For ground-based and laboratory measurements, the VIPS is housed in a sealed canister with a sampling inlet and an outlet equipped with an aspiration fan.

[10] The DVR recorded video at a rate of five frames per second. Freely available software (AVIdemux) was used to extract individual frames from the video files. For the ice fog measurements, the VIPS was equipped with an optical system resulting in a resolution of 1.12 μm per pixel making it possible to detect particles as small as 3 μm under ideal conditions. The collection efficiency of the VIPS has been estimated using calculations based on those of *Ranz and Wong* [1952] for particles larger than 10 μm. The *Ranz and Wong* [1952] calculations predict that only 50% of 10 μm particles would be captured and no particles smaller than 6 μm would be captured. As the VIPS did image particles as small as 3 μm, an empirical collection efficiency curve was determined. To do this, the particle size distributions measured with the VIPS were compared to particle size distributions calculated from the Formvar-coated microscope slides (see below for discussion of Formvar measurements). Empirical collection efficiency values for the VIPS were determined by comparing the observed concentrations in several of the smallest size bins. The ratio of the number of particles in consecutive size bins was determined from the Formvar slides and was compared to the ratio for the same size bins measured by the VIPS. The results of this comparison suggested that the VIPS was undersampling the smallest particles (sub-5 μm) by approximately a factor of 9 and the 5 to 10 μm range by a factor of 2. Figure 2 shows a typical VIPS particle size distribution before and after correction as well as a plot showing the correction factor applied to each size bin. The collection efficiency factors shown in Figure 2b are the values that the observed concentration was multiplied by in order to determine a more realistic value. There is additional uncertainty caused by the fact that VIPS data can only be reasonably separated into size bins that are 5 μm wide due to the resolution. At these small sizes, there is significant
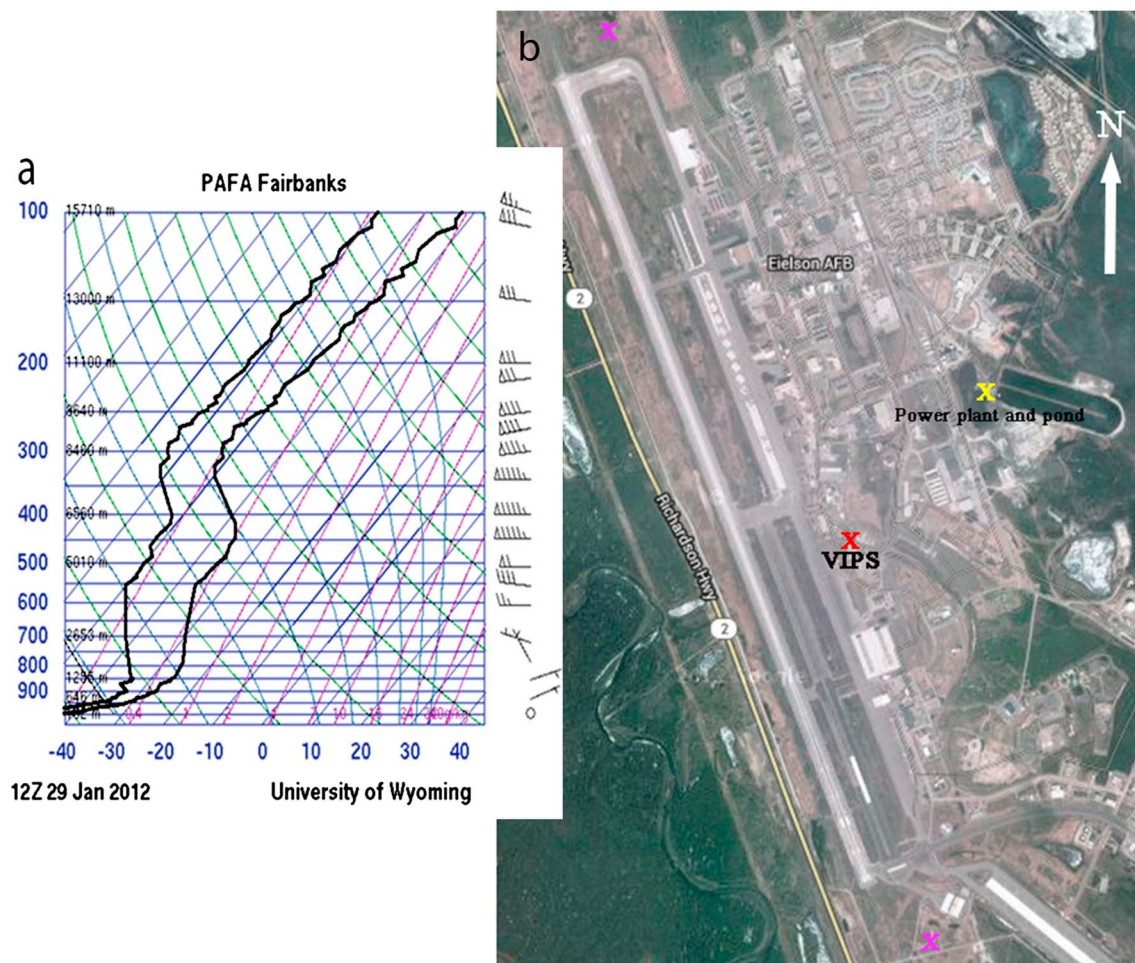
Figure 3. (a) Sounding during heavy ice fog conditions at 4 A.M. local standard time on 29 January 2012. Note the extreme temperature difference near at the surface. (b) Map (maps.google.com) showing the location of the VIPS, the power plant and cooling pond (yellow), and the two Air Force weather stations (magenta).

variation in the collection efficiency of particles at either end of a size bin which could result in significant uncertainty if the peak of the particle size distribution is significantly narrower than the bin width. These collection efficiency results are similar to unpublished results for experiments at the Aerosol Interaction and Dynamics in the Atmosphere cloud chamber under similar conditions (flow rates, 20–50 L/min; particle sizes, 5–50 μm; temperatures, from −30°C to −50°C, etc.) where multiple other particle probes were available for comparisons. The collection efficiency correction for the VIPS measurements led to a near doubling of the total particle concentration (median 88% increase in concentration for the VIPS data set), while the median extinction increase was 27% and the median estimated ice water content increase was 16.5%. The change in the particle size distribution parameters caused by the collection efficiency corrections will be quantified along with the results.

[11] The VIPS aspiration fan speed and the belt movement rate could be varied depending on expected conditions. If higher particle concentrations were expected, the belt speed would be increased to reduce the time of the belt in the sampling inlet. For data analysis, the ideal settings led to approximately 10 particles being in the field of view of each frame which would leave enough space between the particles to get accurate measurements of maximum dimension and projected area while not requiring the analysis of a large number of frames, although results varied significantly, from fewer than one particle (e.g., five particles imaged in 20 frames) being in each frame to more than 500 particles being visible in a frame. The VIPS was mounted on the side of a small trailer with the inlet approximately 1 m above the snow-covered ground with the data system housed in a hard plastic case inside the trailer. The trailer was located in an infrequently used corner of a parking lot approximately 40 m from the nearest road and 200 m from the Eielson Air Force Base (AFB) runway (see Figure 3). During operation, the site was visited daily to change the memory card in the DVR as well as to check the data quality. If necessary, the instrument was returned to the lab for adjustments.

[12] Formvar (polyvinyl formal mixed in a 7.5% by mass solution in chloroform)-coated microscope slides were also used to sample ice fog particles on several occasions. The slides were coated with liquefied Formvar [see *Takahashi and Fukuta*, 1988] and placed on a flat surface to collect falling particles. Collected particles are encapsulated by Formvar which solidifies, producing near-perfect casts of the particles.
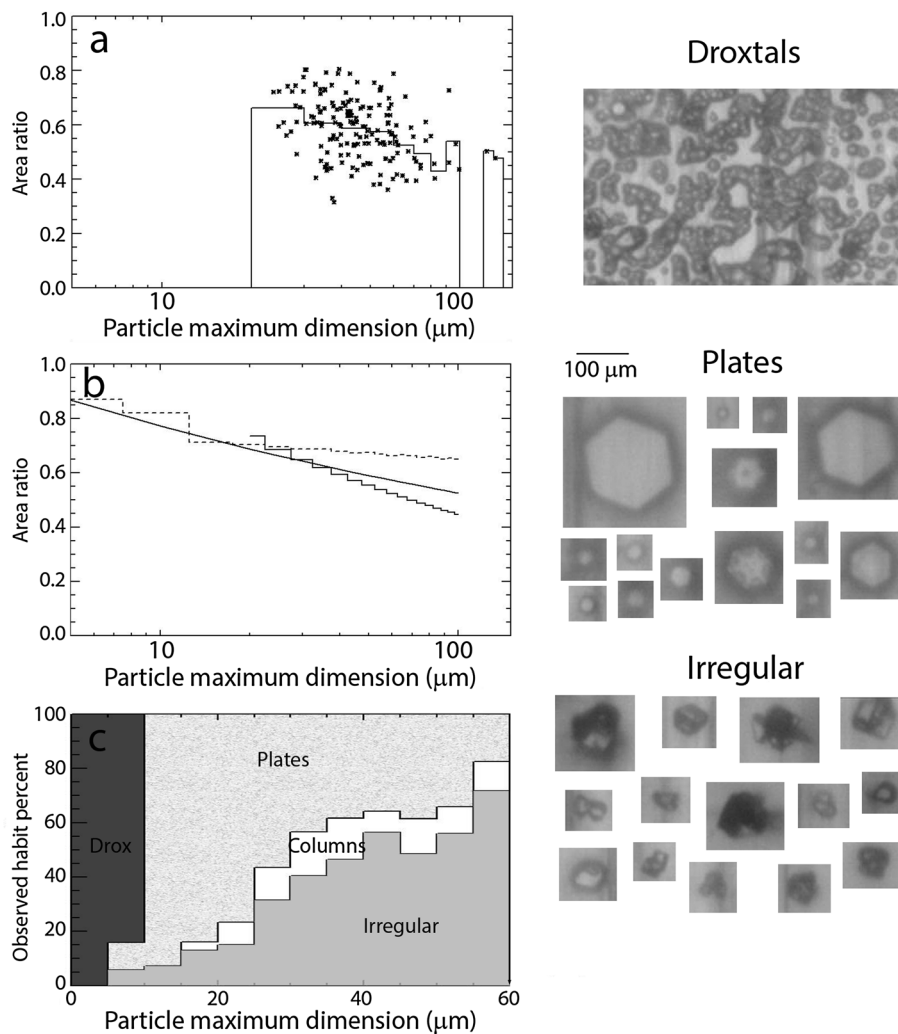
Figure 4. (a) Measured area ratio for irregular particles. Individual particles are indicated with stars, and the median value per size bin is indicated by the solid line. (b) Solid line with steps is a fit to the irregular area ratio values shown in Figure 4a. Dashed line is the expected area ratio for randomly oriented plates of a given aspect ratio. Solid smooth line: fit to average area ratio values based on percentage of each particle size present in each size bin. (c) Percentage of each particle habit observed in 5 μm bins: Dark gray: droxtals. Textured light gray: plate-shaped crystals. White: column-shaped crystals. Smooth light gray: irregular crystals. Example particle images from the VIPS. Droxtals were imaged at 10 UTC on 28 January. Note that the droxtals were not aggregated in the air but only came into contact on the VIPS film. Plate-shaped and irregular-shaped crystals were observed at around 15:00 UTC on 1 February.

Particle replicas in the Formvar were imaged using a Nikon Labofot-2 microscope with a Nikon D-80 digital single-lens reflex (DSLR) camera attached. The DSLR photos had a resolution of approximately 0.42 μm per pixel enabling the measurement of particles as small as 2 μm. Particle size distributions were calculated from ice fog particle replicas by scaling the number of observed particles by the estimated particle terminal velocity calculated using the method of *Heymsfield and Westbrook* [2010]. *Ohtake and Huffman* [1969] used a similar technique for scaling particle size distributions. Formvar-coated microscope slides were used to collect particles if fog was present when the VIPS measurement site was visited as well as during one ice fog event in the city of Fairbanks.

2.2. Analysis

[13] Due to the low contrast between the crystals and the oil-coated tape background (see Figure 4), the image files were hand analyzed. The maximum dimension of each particle was individually measured, and the particles were classified into four categories: plate, column, irregular, and droxtal. For each time period, the first 250 particles from the start of the time period were measured and used to determine the particle size distribution. The measurement of 250 particles was chosen arbitrarily as it produced robust particle size distributions. In instances where the particle habit was nonuniform, the habit of each particle was also noted. The number of frames required to reach 250 was also tabulated, which enabled the calculation of the sample volume. Based on probe
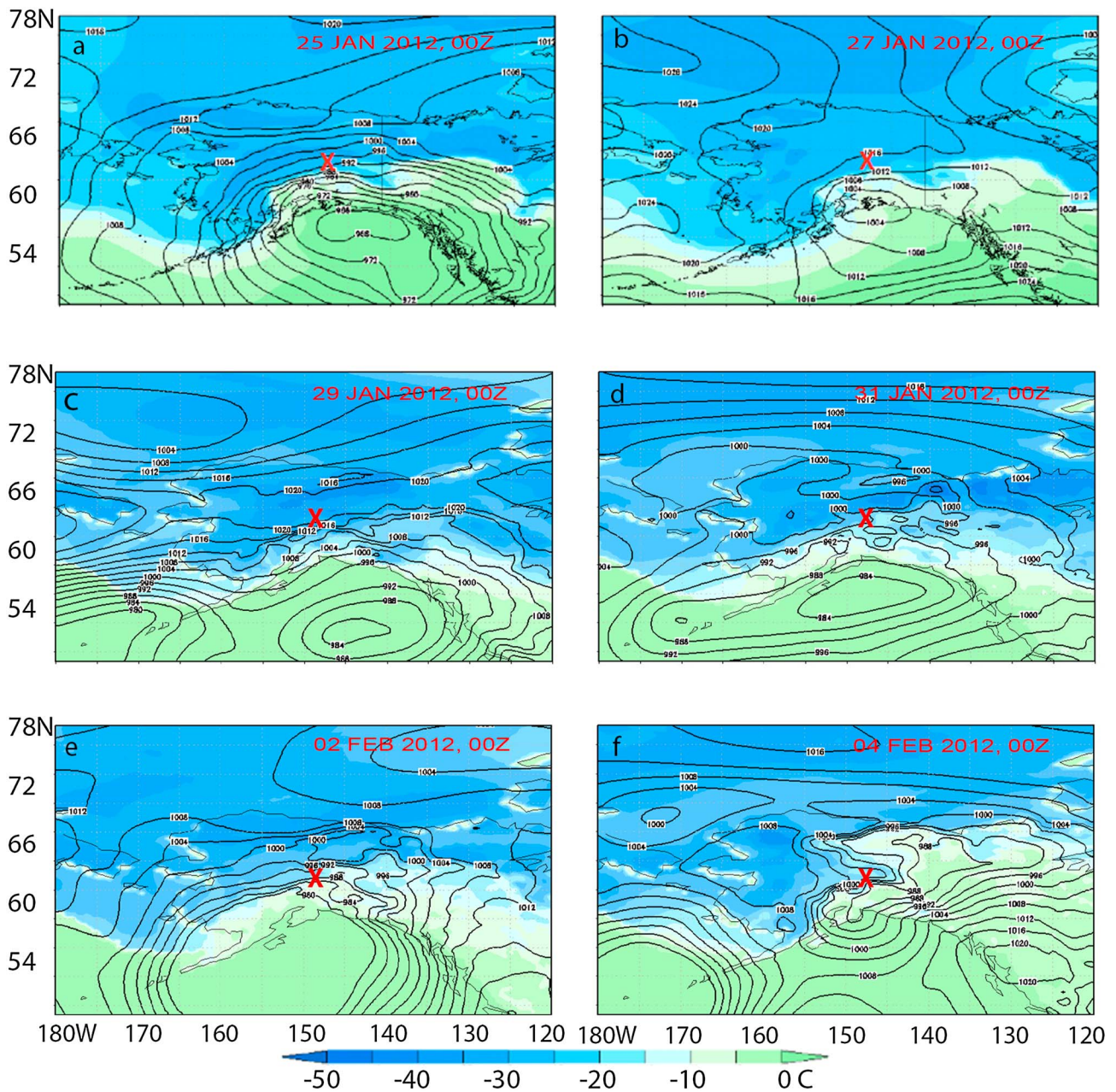
Figure 5. Surface weather maps from 00Z (a) 25, (b) 27, (c) 29, and (d) 31 January and (e) 2 and (f) 4 February 2012. The contour lines indicate the mean sea level pressure (hPa), and the color-coded areas denote the air temperature (°C). The graphics are based on National Centers for Environmental Prediction North American Regional Reanalysis data.

operation and cloud conditions, 250 particles could take anywhere from a few seconds to 15 min to collect. For the 15 VIPS ice fog cases (as defined using the 3 km visibility cutoff), collection times were less than 30 s. Images of irregular particles were also saved for later processing to determine the projected area to maximum dimension relationship. In total, more than 10,000 crystals were hand measured and classified, and an additional 10,000 were counted for concentration time series calculations. *Hallett* [2003] suggests that Poisson statistics indicate that the uncertainty in ice crystal size distributions due to random sample error are proportional to the square root of the number of counts for each bin. For ice fog

size distributions developed from 250 particles, generally, the uncertainty per bin ranged from 8% to 20% for 60% of the bins with more than a few counts.

[14] For the analysis of the Formvar slides, as with the VIPS data, 250 particles were measured, and particle habits were tallied for each measurement. Since Formvar dries at different rates depending on the conditions as well as the application thickness, the particle size distributions could not be scaled without external information. Unscaled particle size distributions were scaled by the estimated particle fall speeds to determine the relative concentrations of each size bin. This technique requires that the sites be completely calm which
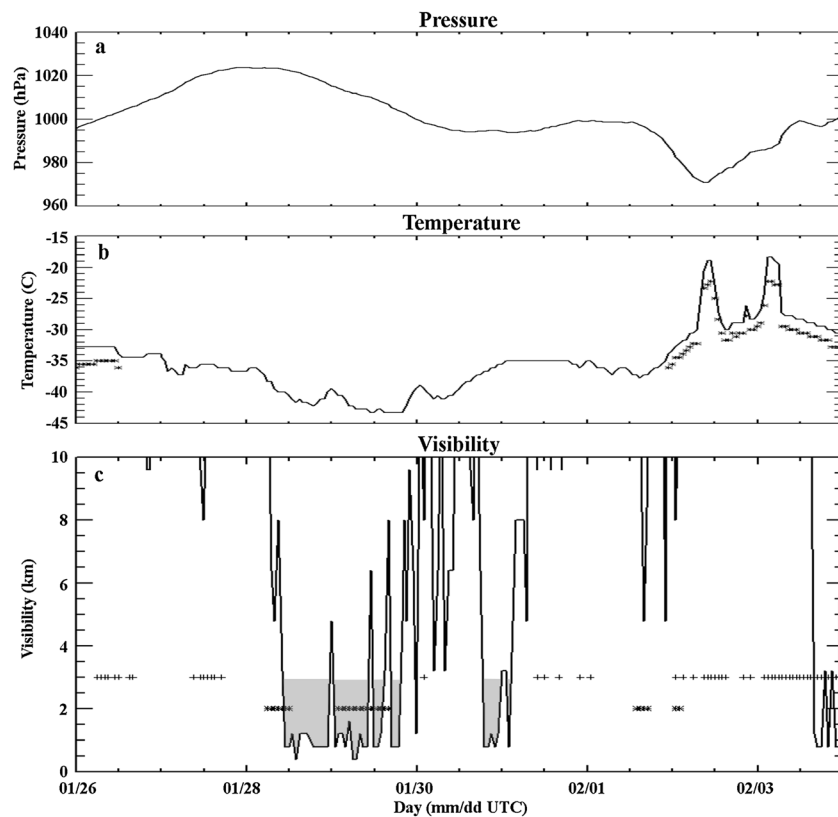
Figure 6. Time series of (a) mean sea level pressure, (b) temperature, and (c) visibility measured at the Eielson Air Force Base from 26 January to 4 February 2012 showing the development conditions leading to the development of the ice fog. Stars in Figure 6b indicate the dew point temperatures. Dew point temperatures were not reported when values were lower than $-36°C$ as they were considered to be unreliable. Times when the wind measurement was above the instrumentation detection threshold are indicated by plus signs at the 3 km visibility level in Figure 6c. Time periods when the VIPS data was analyzed are indicated by stars at the 2 km visibility level. The shaded regions in Figure 6c indicate the time periods which were considered to be ice fog while other reductions in visibility were likely significantly influenced by diamond dust.

was true during all ice fog observations as reported by the National Weather Service. The local visibility measurements provided by the Air Force to the National Weather Service were used to scale the absolute values of the Formvar size distributions, although significant uncertainty exists as the measurements were not colocated.

3. Synoptic Conditions

[15] Between 26 January and 4 February 2012, there were several ice fog events in the Fairbanks area. At the Eielson Air Force Base, the visibility was below 3 km for a total of 42 h spread over three main episodes. As expected, the ice fog developed on nights when the skies were clear and the surface was able to radiatively cool. A typical sounding from a particularly strong ice fog event is shown in Figure 3a. The temperature 150 m above the surface was 10°C warmer than at the surface. Figure 3b shows a map with the location of the measurement site. A power plant with an open water cooling pond was located near the measurement site. The Air Force operates two Coastal Environmental (http://www.coastalenvironmental. com) FMQ-19 fixed base weather stations located at each end of the runway (Figure 3b). The Air Force collects the data and makes them available to the National Weather

Service. The NWS data available include temperature, air pressure, wind speed and direction, relative humidity, visibility, and cloudiness.

[16] A low-pressure area located in the Gulf of Alaska and a high-pressure system over Interior and north Alaska characterized the general weather in Alaska the last 5 days of January 2012 at the beginning of our observational period (see Figure 5). Only very small horizontal pressure gradients in Interior Alaska account for no or very weak surface winds during most times from the end of January to February 2012. During our observational period, high-pressure and weak horizontal gradients remained in Interior Alaska except for a short period from 3 to 4 February 2012, when the surface pressure decreased with the advection of warmer air from the southeast.

[17] Six hours before the onset of the ice fog (00 UTC 28 January 2012), high-pressure and minimal surface gradients dominated the synoptic situation over Fairbanks. This weather situation is similar to the conditions necessary for ice fog development described by *Bowling et al.* [1968]: migratory high-pressure moves from Siberia across Alaska, which lead to a high-frequency of occurrence of ice fog in Fairbanks. A surface inversion with a temperature lapse rate of 10.9°C $(100 \, m)^{-1}$ was observed 6 h before the onset of ice fog

(00 UTC, 28 January 2012). During the ice fog event from 29 to 30 January 2012, the surface inversion persisted with a slightly weaker intensity (4.2–6.0°C (100 m)$^{-1}$). *Kim and Yum* [2012] have indicated that the outgoing longwave radiation at the top of the fog layer can induce a slight lifting of the top of the fog layer. Figure 6 shows a time series of the temperature T, mean sea level pressure, and visibility derived from METAR observations at the Eielson Air Force Base. Also plotted in Figure 6c, the stars at the 2 km visibility level indicate the times when the VIPS was operating and data were analyzed. The plus marks at the 3 km visibility level indicate times when the winds were above the minimum detectable winds. T gradually decreases with some fluctuations as the migratory anticyclone approaches Fairbanks. The air still cools to the minimum T of −46.5°C even as the mean sea level pressure decreases. Then, T increases to −30°C during the fog dissipation stage.

4. Microphysical Measurements

[18] The VIPS was operated at Eielson AFB nearly continuously during the 26 January to 4 February ice fog events when the observed visibility dropped to as low as 0.8 km. From initial setup to final takedown, the VIPS was in operation for 109 h and in the shop for maintenance or in transportation for 97 h. Due to various suspected instrument issues, 33 h of data were deemed unreliable. Particle size distributions were determined from the VIPS measurements every 30 to 60 min during 27 h of measurements. For most of the remainder of the time, there was no fog present on site. During all observations at the Eielson Air Force Base, the wind speed data only showed one measurement at the instrument detection threshold (equal to ~1.5 m/s); otherwise, the wind speed was always below the detection threshold of the instrumentation (see the plus signs on Figure 6c). The VIPS data were not analyzed during the period when the winds were detected. Cloud extinction and ice water content were calculated based on the particle size distributions and the habit estimates. Figure 4 shows the breakdown of particle habits for all of the observations. Generally, particle habits were similar for all measurements when separated by particle size. During all observations, most of the observed particles smaller than 10 μm were quasi-spherical droxtals. When larger particles were present, they fell into the categories by percentages shown in Figure 4c regardless of the optical thickness of the cloud. For ice fog cases, particles were rarely larger than 50 μm, meaning that the characteristics estimated for irregular particles rarely had a substantial influence on ice fog calculations. The particle images shown in Figure 4 represent typical particles of those habits imaged by the VIPS. The droxtal image is from a very dense fog time period leading the particles to come into contact after landing on the VIPS tape.

[19] The particle size distributions and average particle projected area for particle sizes were integrated to produce a bulk extinction value for visibility comparisons. To calculate accurate extinction values, it was necessary to estimate the projected area of individual particles, which is not necessarily the projected area imaged by the VIPS. *Breon and Dubruelle* [2004] noted that particles with Reynolds numbers below 0.39 have no preferred orientation during falling. Based on mass, maximum dimension, and area estimates, the 0.39 Reynolds number cutoff for the observed ice fog

particles occurred at ~75 μm for the local temperature and pressure conditions (−40°C and ~1000 mbar). To calculate the average projected area of a randomly oriented hexagonal plate, a computer program developed for *Schmitt and Heymsfield* [2010] was used to create theoretical hexagonal crystals of known dimensions which were rotated randomly in three dimensions. As it was impossible to measure both dimensions (the *a* and *c* axes) of plate-shaped crystals from VIPS imagery, an equation derived by *Schmitt and Arnott* [1999] under similar conditions (−18°C ± 3°C, 900 hPa, and particle concentrations on the order of several units per cm^3) in the laboratory was used to estimate the thickness of plate-shaped crystals. Their equation is C = 0.74 * D$^{0.7}$, where C is the plate thickness and D is the plate maximum dimension. For column-shaped crystals, both axes can be measured, and it was noted that for the measured columns, the length was typically 1.5 times the width with no dependence on particle size. For each set of crystal dimensions, the projected area was calculated for 5000 random orientations, which were then averaged to determine an average projected area for a randomly oriented crystal in the atmosphere. For irregular-shaped crystals, the area ratio (the projected area of the particle divided by the area of the smallest circle that will completely hide the particle) of a selection of particles was determined, and average values were calculated for each size bin. Figures 4a and 4b show the area ratio calculated for each of the different habit categories. As particle habits did not vary much by cloud type, this information was used to determine an area ratio relationship used for all extinction calculations. For each size range, a weighted average was calculated of the observed area ratios based on the area ratio and percentage of each habit present in that size range. An extinction efficiency of 2.0 was assumed when converting total projected area to extinction. Given the very small size of particles at times, the integrated extinction efficiency could be as high as 2.2 based on Mie theory calculations had the particles been spheres.

[20] The average mass of the observed ice fog particles was estimated in a similar way to the area. The mass of droxtal-shaped ice particles and hexagonal crystals was estimated by geometry [*Yang et al.*, 2003]. As it is not possible to determine the mass of irregular particles from two-dimensional images, we initially assumed that irregular particles had the same mass as the hexagonal plates of the same maximum dimension. Varying the mass of irregular particles from zero to the mass of ice spheres had little effect on ice water content calculations for ice fog. The area dimensional relationship and the mass dimensional relationship are shown in equations 1 and 2. Equations 1 and 2 are expressed in terms of particle area ratio and particle density (the three-dimensional analogy of area ratio: the mass of the particle divided by the mass of a unit density sphere of equal maximum dimension).

$$A_r = 1.0 * D^{-0.12} \tag{1}$$

$$\rho = 0.91 * D^{-0.35} \tag{2}$$

[21] A_r is the particle area ratio, D is particle maximum dimension (in μm), and ρ is density. These parameterizations were slightly adjusted from the directly calculated mathematical fits so that solid ice spheres would result for 1 μm particles. When area ratio values are calculated using equation 1, the
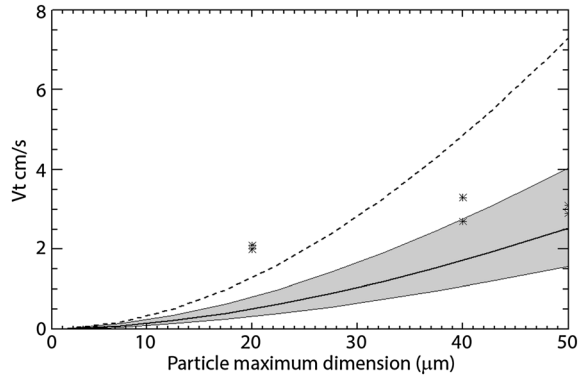
Figure 7. Particle terminal velocity calculated with area and mass assumptions described in text. Bold line is the value expected by particle size. The shaded area delineates a −40% to +60% range based on applying minor perturbations to mass and area values. Dashed line is the calculated value for spherical ice particles (density: 0.91 g/cm^3). Stars represent laboratory measurements of particle terminal velocity by Kajikawa (1973) at warmer temperatures (−10°C to −15°C). Stars at 20 μm are for mean values of columns and plates together, those at 40 μm are for columns, and those at 50 μm are for plates.

results are within 5% of the average values calculated by assuming the particle habit distribution shown in Figure 4 for particles smaller than 50 μm. For larger particles, the area ratio uncertainty increases up to 25% at 100 μm. For uncertainty calculations later in this manuscript, an uncertainty of ±25% is assumed for projected area estimates. As there are no true mass measurements for sub-100 μm atmospheric ice cloud particles, the uncertainty in equation 2 is assumed to be ±50% with an upper limit being placed at the mass of an ice sphere with the same maximum dimension.

[22] With equations 1 and 2, it is possible to estimate particle terminal velocity using the *Heymsfield and Westbrook* [2010] formulations. Figure 7 shows the terminal velocity estimated for ice fog particles. Uncertainty estimates were made by recalculating particle terminal velocity with projected area and mass value perturbations at the upper and lower ranges that could be expected based on the observations as described above. The resulting estimates show that the shaded uncertainty range is approximately from −40% to +60% by using the combination of mass and area uncertainties that lead to the largest uncertainty in calculated terminal velocity. Stars on the figure represent mean values of terminal velocity measured by *Kajikawa* [1973] for differing particle shapes under slightly warmer atmospheric conditions. The shapes
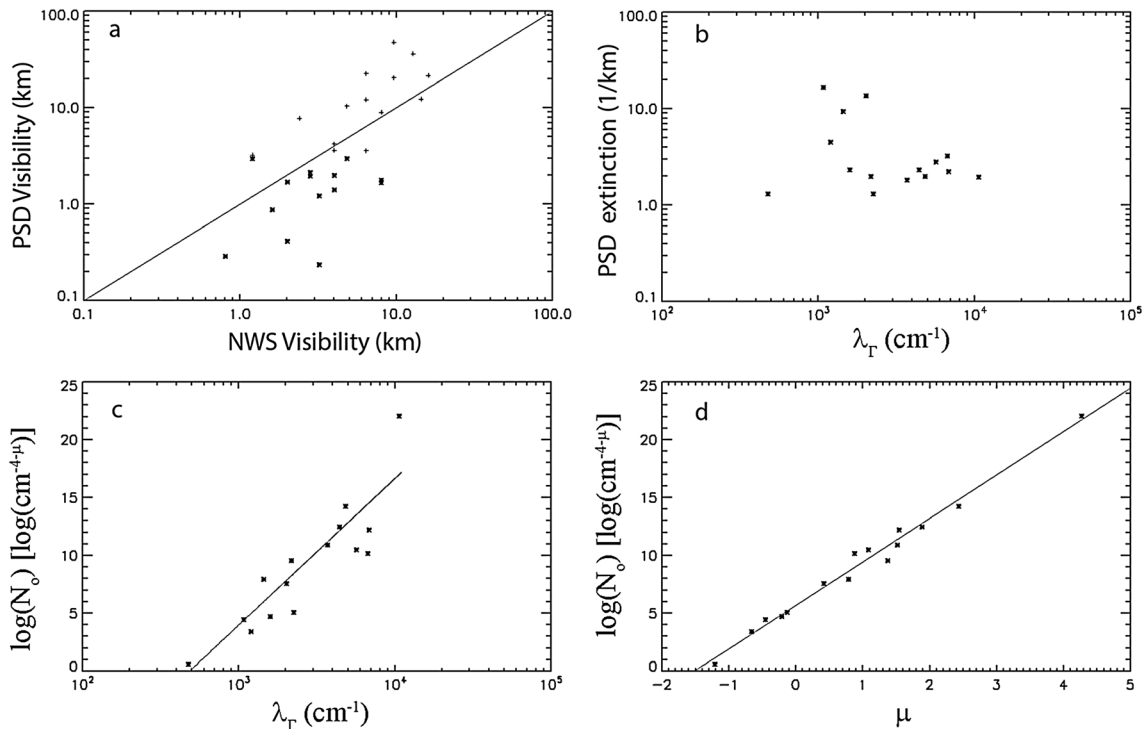
Figure 8. Particle size distribution properties from the ice fog data set. Each point measurement represents the properties calculated from a particle size distribution measured when the visibility was less than 3 km as determined by the VIPS. (a) The visibility calculated from the particle size distributions compared to the measured visibility. The 1 to 1 line is drawn for guidance. Stars represent the VIPS measurements in ice fog. Also shown in Figure 8a are visibility calculations for time periods when the visibility was higher than the 3 km cutoff (represented by plus signs). (b) Extinction versus PSD slope lambda showing no trend. (c) λ_Γ versus log (N_o). (d) log (N_o) versus μ. Fits for Figures 6c and 6d are given in equations 4 and 5.

Table 1. Microphysical Parameters for the Normalized Mean Particle Size Distributions for Ice Fog at Two Sampling Locations

Property	Eielson AFB	Uncertainty Factor	Fairbanks
Visibility (km^{-1})	0.78 ± 0.5	0.63 ± 0.16	1.01 ± 0.6
Temperature (°C)	-43.1 ± 2.4		-44.3 ± 1.1[a]
Total concentration (cc)	33		68
λ_Γ (cm^{-1})	1000	0.91 ± 0.11	2500
μ	-0.8	$(\mu+2)$, 0.75 ± 0.13[b]	-0.64
No (cm$^{-4-\mu}$)	580	(log(No)), 0.78 ± 0.11[b]	2200

[a]During the night when the Fairbanks Formvar measurements were taken, the chloroform and Formvar solution froze indicating that the temperature was significantly colder than the temperature reported by the NWS approximately 3.4 km away.

[b]Uncertainty factors for μ and N_o are in the units plotted in Figure 9.

from *Kajikawa* [1973] are indicated in the figure caption. The dashed line shows the terminal velocity estimated for ice spheres for comparison. Given that the terminal velocity of 20 µm ice fog particles is less than 1 cm/s, it is not surprising that ice fog persists for long time periods. A fit to the terminal velocity curve is given in equation 3.

$$V_t = 0.0027 * D^{1.73} \qquad (3)$$

[23] The data used to construct Figure 7 and equation 3 assume a temperature of -40°C and an atmospheric pressure of 1000 hPa. *Heymsfield et al.* [2013] presented an improved method for adjusting terminal velocity estimates to different temperature and pressure regimes, although it should be stressed that these results are for ice fog and should not be used for other cloud types.

[24] Figure 8 shows observed ice fog microphysical relationships for the ice fog particle size distributions measured during the ice fog cases using the less than 3 km of visibility cutoff. In all, values were derived from 21 particle size distributions, 15 from VIPS data from the Eielson Air Force Base and 6 from Formvar samples collected in Fairbanks. Fog extinction was calculated by summing the projected area over the particle size distribution using 1, and then converting to visibility using the Koschmieder equation [*Koschmieder*, 1924]. Thus, $Vis = 3.912/\sigma$, where σ is the extinction (the units of visibility depend on the units of σ). Figure 8a shows the relationship between the calculated visibility and the visibility measured at the Eielson AFB site. Only data points shown for the VIPS are shown in Figure 8a as the Formvar measurements were scaled by the visibility measurements. The stars represent times when the 3 km visibility limit was reached according to the VIPS calculations. The plus signs indicate visibility calculated from other time periods when the visibility was higher than 3 km. The plus signs are shown to indicate that, though there was significant scatter, the trends are reasonable over a significant range of values (0.8 km to 16 km). The scatter is likely due to the fact that the VIPS and the weather stations were not colocated and the plume from the power plant could easily impact one and not the other. Figure 1b can help to understand the extreme local variability, as when the photo in Figure 1b was taken, it was nearly perfectly clear approximately 3 km to the east at the Eielson AFB entrance station. While the lower level winds were below the detection threshold of the Air Force instrumentation for all VIPS time periods analyzed, upper level winds (at the height of the power plant stack) could be seen to shift slowly with time. Given the location of the instrumentation (Figure 3), it is easily conceivable that the plume could drift over the VIPS leaving the Air Force instruments in the clear or the VIPS in the clear while the Air Force instruments were in fog. The VIPS was located 1.1 km from the power plant and 2.95 and 1.95 km from the weather stations at the north and south ends of the runway, respectively. The weather stations are equidistant from the power plant, approximately 2.8 km
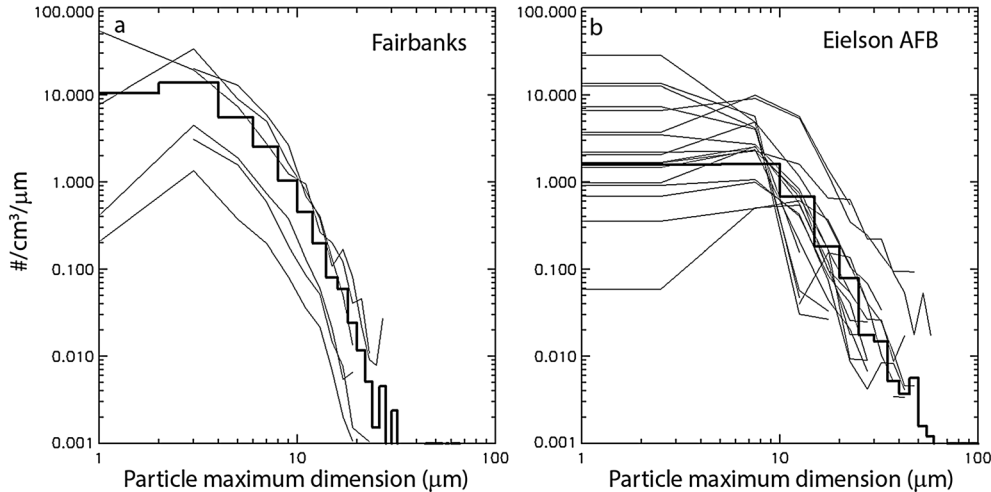
Figure 9. Particle size distributions for the two different measurement locations. Thin lines are the individual particle size distributions measured at each location when the visibility was less than 3 km. Bold line is the average of the particle size distributions after they were normalized to 1.6 km visibility. Eielson AFB measurements are from the VIPS, which had a 5 µm bin width while a 2 µm bin width was used for the Fairbanks measurements from Formvar collections. Gamma distribution parameters for the averaged distributions are shown in Table 1. Note the wide range of values in the first bin. Uncertainty estimates in Table 1 include the differences associated with ignoring the collection efficiency estimates.

distant. The fact that the VIPS was located closer to the power plant than either of the weather station likely accounts for why the VIPS visibility was often lower than the weather station measured visibility.

[25] The particle size distributions were fit to gamma distributions of the form $N(D) = N_o D^\mu \exp^{-\lambda_\Gamma D}$, where N_o is the intercept, λ_Γ is the slope, and μ is the dispersion. These parameters are plotted with respect to other more easily derived parameters in Figures 6b–6d. Figure 8b shows that the λ_Γ-σ (extinction) relationship appears to have no trend. Since the gamma fit is optimized to match the second, third, and sixth moment of the size distribution [*Heymsfield et al.*, 2002], the occasional large particle causes a significant change in λ. Figure 8c shows the λ_Γ-N_o relationship. Equation 4 gives a relationship for the fit line shown in Figure 8c. Figure 8d shows the relationship between N_o and μ, and a parameterization is given in equation 5.

$$\log(N_o) = 0.0071\lambda_\Gamma{}^{0.88} \qquad (4)$$

$$N_o = 0.0145 * \exp[8.66(\mu + 2)] \qquad (5)$$

Uncertainties for the above equations are shown in Table 1 for the data set.

[26] Figure 9 shows a comparison between typical particle size distributions measured at Eielson AFB and the Formvar measurements taken in Fairbanks during the night of 29–30 January. These data were notable because the visibility measured at Fairbanks International Airport was significantly lower than at the Eielson Air Force Base with values as low as 0.2 km being reported during the night. The particle size distributions determined from the Fairbanks Formvar slides were scaled by the local measured visibility. Slides were placed out every 2 h through the night during the heaviest ice fog episode, but only data from the evening and the following morning were usable, as the chloroform and Formvar mixture froze during the coldest part of the night. As the freezing temperature of chloroform is −63.5°C, this suggests that the temperature may have been locally colder than the low of −47°C that was recorded at the airport 3.4 km away. Individual lines shown in each figure represent individual particle size distributions while the bold lines represent the average particle size distributions. Data are included when the visibility was reported as less than 3 km. The average particle size distributions were determined by first normalizing the size distributions to a visibility of 1.6 km (arbitrarily chosen) so that each distribution was treated similarly. The parameters for the gamma fits to the averaged particle size distributions are shown in Table 1. Also shown in Table 1 are uncertainty factors for the VIPS measurements based on the collection efficiency corrections. Size distribution parameterizations were calculated with and without the collection efficiency adjustments. The mean uncertainty shown in the uncertainty column represents the mean ratio of the collection efficiency corrected value divided by the uncorrected value. The associated uncertainty is the standard deviation of the obtained ratio values. The uncertainties for N_o and μ are in the form in which the parameterizations are presented [e.g., $\log(N_o)$ and $(\mu + 2)$] in equations 4 and 5.

[27] The results shown here are meant to be useful for characterization of ice fog microphysical properties in polluted conditions. When the visibility was greater than 3 km, the influence of diamond dust particles increased. The Fairbanks

measurements can be considered to be from a heavily polluted area as they were collected near an airport, a highway, and a major shopping area where it was observed that customers generally left their cars running while they shopped. The Eielson AFB measurements while in a less heavily trafficked area should still be considered to be from a polluted environment and may have been influenced by the open water cooling pond. The higher level of pollution at the Fairbanks site is shown in the higher particle concentration as well as the narrower particle size distribution (λ_Γ of 2500 in Fairbanks versus 1000 at Eielson AFB).

5. Summary

[28] For the first time in several decades, ice fog particle observations are reported for Interior Alaska region. In the Fairbanks, Alaska region, ice fog forms easily on cold (−30°C and colder) clear nights due to high levels of emissions of particulates and water vapor from anthropogenic sources. The Video Ice Particle Sampler probe was used to continuously collect ice particles near the surface in a highly impacted region. Particle size distributions were determined from VIPS measurements and visibility was estimated. Microscope slides coated with liquefied Formvar were also used to calculate particle size distributions. A visibility limit of 3 km was used to separate ice fog events from non-ice fog time periods. The Formvar slide results indicated that the peak of the particle size distribution was typically in the 2–4 μm range which is at the low end of peak sizes previously reported. This is likely due to the extremely high pollution levels present at the Fairbanks observation site. For the VIPS measurements at the Eielson Air Force Base, the peak of the measured size distributions was between 5 and 10 μm, although this size range has increased uncertainty due to multiple issues.

[29] Measured particle sizes were generally very small (less than 30 μm) during ice fog events, while during non-ice fog periods, larger diamond dust crystals up to 150 μm were observed. Most particles smaller than 10 μm were quasi-spherical droxtal-shaped faceted ice crystals while larger crystals were more likely to be plate-shaped with irregular crystals becoming more common at sizes larger than 30 μm. Column-shaped ice crystals were rarely observed. Particle projected area dimensional and mass dimensional relationships have been developed for the particle populations as well as particle terminal velocity estimates.

[30] The results of this study are being used in a follow up study to improve the ability of the WRF model to predict the onset and longevity of ice fog under polluted conditions.

References

Benson, C. S. (1970), ICE FOG, *Weather*, *25*(1), 11–18.
Bowling, S. A., T. Ohtake, and C. S. Benson (1968), Winter pressure systems and ice fog in Fairbanks, Alaska, *J. Appl. Meteorol.*, *7*, 961–968.
Breon, F.-M., and B. Dubruelle (2004), Horizontally oriented plates in clouds, *J. Atmos. Sci.*, *61*, 2888–2898.

Curry, J. A., F. G. Meyer, L. F. Radke, C. A. Brock, and E. E. Ebert (1990), Occurrence and characteristics of lower tropospheric ice crystals in the arctic, *Inter. J. Climatology*, *10*(7), 749–764.

Girard, E., and J.-P. Blanchet (2001), Microphysical parameterizations of arctic diamond dust, ice fog, and thin stratus for climate models, *J. Atmos. Sci.*, *58*, 1181–1198.

Gultepe, I., G. Pearson, J. A. Milbrant, B. Hansen, S. Platnick, P. Taylor, M. Gordon, J. P. Oakley, and S. G. Cober (2009), The fog remote sensing and modeling field project, *Bull. Am. Meteorol. Soc.*, *90*, 341–359.

Hallett, J. (2003), Measurement in the atmosphere, in *Handbook of Weather, Climate and Water: Dynamics, Climate, Physical Meteorology, Weather Systems, and Measurements*, edited by T. D. Potter and B. R. Colman, pp. 711–720, Wiley-Interscience, Hoboken, NJ.

Heymsfield, A. J., and C. D. Westbrook (2010), Advances in the estimation of ice particle fall speeds using laboratory and field measurements, *J. Atmos. Sci.*, *67*, 2469–2482, doi:10.1175/2010JAS3379.1.

Heymsfield, A. J., A. Bansemer, P. R. Field, S. L. Durden, J. L. Stith, J. E. Dye, W. Hall, and C. A. Grainger (2002), Observations and parameterizations of particle size distributions in deep tropical cirrus and stratiform precipitating clouds: Results from in-situ observations in TRMM field campaigns, *J. Atmos. Sci.*, *59*, 3457–3491.

Heymsfield, A. J., C. Schmitt, and A. Bansemer (2013), Ice cloud particle size distributions and pressure dependent terminal velocities from in situ observations at temperatures from 0 to -86C, *J. Atmos. Sci.*, doi:10.1175/JAS-D-12-0124.1, accepted.

Kajikawa, M. (1973), Laboratory measurements of falling velocity of individual ice crystals, *J. Meteorol. Soc. Japan*, *51*, 263–271.

Kim, C., and S. Yum (2012), A numerical study of sea-fog formation over cold sea surface using a One-Dimensional Turbulence Model coupled with the Weather Research and Forecasting Model, *Boundary-Layer Meteor.*, *143*, 481–505.

Koschmieder, H. (1924), Theorie der horizantalen sichtweite, *Beitr. Phys. Atmos.*, *12*(33-55), 171–181.

Kumai, M. (1966), Electron microscopic study of ice-fog and ice-crystal nuclei in Alaska, *J. Met. Soc. of Japan. Ser. II*, *44*(3), 185–194.

McFarquhar, G. M., and A. J. Heymsfield (1997), Parameterization of tropical cirrus ice crystal size distributions and implications for radiative transfer: results from CEPEX, *J. Atmos. Sci.*, *54*, 2187–2200.

Ohtake, T., and P. J. Huffman (1969), Visual range in ice fog, *J. Appl. Meteorol.*, *8*, 499–501.

Ranz, W. E., and J. B. Wong (1952), Impaction of dust and smoke particles on surface and body collectors, *J. Ind. Eng. Chem.*, *44*, 1371–1381.

Schmitt, C. G., and W. P. Arnott (1999), Infrared emission (500-2000 cm-1) of laboratory ice clouds, *J. Quant. Spectros. Radiat. Transfer*, *63*, 701–725.

Schmitt, C. G., and A. J. Heymsfield (2009), The size distribution and mass-weighted terminal velocity of low-latitude cirrus crystal populations, *J. Atmos. Sci.*, *66*, 2,013–2,028, doi:10.1175/2009JAS3004.1.

Schmitt, C. G., and A. J. Heymsfield (2010), Dimensional characteristics of ice crystal aggregates from fractal geometry, *J. Atmos. Sci.*, *67*, 1605–1616, doi:10.1175/2009JAS3187.1.

Schön, R., M. Schnaiter, Z. Ulanowski, C. Schmitt, S. Benz, O. Mohler, S. Vogt, R. Wagner, and U. Schurath (2011), Particle habit imaging using incoherent light: A first step toward a novel instrument for cloud microphysics, *J. Atmos. Oceanic Technol.*, *28*, 493–512, doi:10.1175/2011JTECHA1445.1.

Takahashi, T., and N. Fukuta (1988), Ice crystal replication with common plastic solutions, *J. Atmos. Oceanic Technol.*, *5*, 129–135.

Thompson, G., R. M. Rasmussen, and K. Manning (2004), Explicit forecasts of winter precipitation using an improved bulk microphysics scheme, Part I: Description and sensitivity analysis, *Mon. Weather Rev.*, *132*, 519–542.

Thuman, W. C., and E. Robinson (1954), Studies of Alaskan ice-fog particles, *J. Appl. Meteorol.*, *11*, 151–156.

Wendler, G. (1969), Heat balance studies during an ice-fog period in Fairbanks, Alaska, *Mon. Weather Rev.*, *97*, 512–520.

Yang, P., B. A. Baum, A. J. Heymsfield, Y. X. Hu, H.-L. Huang, S.-C. Tsay, and S. Ackerman (2003), Single-scattering properties of droxtals, *J. Quant. Spectros. Radiat. Transfer*, *79-80*, 1159–1169.